COBEM 2023 27TH INTERNATIONAL CONGRESS OF MECHANICAL ENGENEERING

ABCM Brazilian Society of Mechanical Sciences and Engineering
27th ABCM International Congress of Mechanical Engineering
December 04-08, 2023, Florianópolis-SC, Brazil

COB-2023-1877
ON THE DYNAMIC BEHAVIOUR OF FINITE AND INFINITE BEAMS WITH LUMPED PARAMETER ATTACHMENTS

Jean Paulo Carneiro Jr.
Paulo José Paupitz Gonçalves
Michael John Brennan
State University of São Paulo – School of Engineering, Bauru – Brazil
jean.carneiro@unesp.br, paulo.paupitz@unesp.br, mjbrennan0@binternet.com

Vladislav Sorokin
The University of Auckland – Acoustics Research Centre, Auckland – New Zealand
v.sorokin@auckland.ac.nz

Vinicius Germanos Cleante
Aeronautics Institute of Technology – Division of Mechanical Engineering, São José dos Campos – Brazil
cleante@ita.br

Brian Mace
Donovan du Toit
The University of Auckland – Acoustics Research Centre, Auckland – New Zealand
b.mace@auckland.ac.nz, ddut037@aucklanduni.ac.nz

Abstract. *There is a growing number of structural design forms favouring unorthodox and/or very slender structures. Many studies have been dedicated to methods for modelling and mitigating vibrations in such systems. A simple way to analyse vibration control alternatives in slender structures is to model them as one-dimensional waveguides. Among the methods applied in such analyses, wave-based approaches are widely found in the literature. Still, they are often restricted to infinite systems, which leads to obscure the relationship with the behaviour of finite structures. This work describes the propagation of vibration in infinite and finite slender beams, with attached force and moment type discrete elements. Using the wave approach, the transmission coefficient of an infinite beam with general dynamic stiffness attached is assessed. From the dynamic stiffness and receptance matrix method, the displacement transmissibility of a finite beam is obtained, allowing the direct prediction of the behaviour of slender systems with attached discrete dynamic stiffness elements. Numerical results discuss the effects of coupling a pure moment inertia and a translational grounded spring to the beam. The analysis shows the formation of an ultra-wide attenuation band, due to the correct tuning of the local resonance effect. Experimental procedures were conducted to support the theoretical discussions, showing good agreement between the results.*

Keywords: *vibration suppression, force-moment devices, transfer matrix method, displacement transmissibility.*

1. INTRODUCTION

Modern structural designs consider multiple factors associated with the application. In civil engineering, there is a growing number of architectural design forms favouring unorthodox and/or very slender structures, which require dynamic analyses, far beyond the traditional statics only considerations (Meskouris et al., 2019). In this context, many studies have been dedicated to methods for modelling and mitigating vibrations, often induced by wind or seismic excitation (Jafari and Alipour, 2021; Jiménez-Alonso et al., 2020). An example of the latter was the application of local resonance systems to reduce vibration from directional waves, promoting significant filtering characteristics and relatively deep bandgaps at low frequencies (Kalderon et al., 2022). These issues have particular relevance to aerospace applications, where it is not uncommon to find works in which authors concentrate their efforts on mitigating the vibration transmitted from the launch vehicle to the satellite through structural changes in the transmission path (Chen et al., 2020).

A simple way to analyse vibration control alternatives in structures is to model them as one-dimensional waveguides. This approach provides the deep physical interpretation needed to support more complex analyses. Classic examples of one-dimensional waveguides are rods and beams. Fairly extensive studies on these systems in the literature often assume them to be infinite. On transverse waves in beams, the textbooks (Cremer et al., 2005; Mead, 1982; Mead, 1998) contain the fundamental theoretical summary on the subject.

In the early investigations, (Mace, 1984) describes the reflection and transmission matrices in infinite beams. An analytical and experimental investigation of the control of flexural waves with a tuneable vibration absorber is described by (Brennan, 1999). The presented discussions demonstrate the resonant interaction between the device and the beam, and the effect of damping on the bandwidth. Recently, an infinite beam with a point discontinuity consisting of uncoupled force- and moment-type vibration neutralisers was investigated analytically by (Toit et al., 2021). The results indicate the potential for transmission reduction when applied resonators act on both types of motions.

The aforementioned works, as many others found in the literature, focus on the evaluation of infinite systems. These approaches provide deep physical insights, however in practical cases, in finite structures, other phenomena must be considered. The present work aims to expand the discussions and describe the dynamic behaviour of a finite slender beam with concentrated elements with moment- and force- types of action, based on the analysis of infinite systems.

The paper is organised as follows. Section 2 develops the theoretical foundations and general discussions about wave transmission in infinite beams. In Section 3, the dynamic stiffness matrix method is applied to a finite beam and is discussed with reference to the preceding section. Practical advantages in terms of vibration attenuation are presented with the condition for forming an ultra-wide attenuation band. The theoretical analysis is validated in Section 4, in which a series of experimental demonstrations is presented. Finally, in Section 5, the conclusions of this work are outlined.

2. BACKGROUND: SUPPRESSING INCIDENT WAVES ON AN INFINITE BEAM

Figure 1 shows an infinite beam, with cross-sectional area S, second moment of area I, Young's modulus E and density ρ. A source distant to the left generates a propagating incident wave, denoted by the wave amplitude A_i, which travels until it finds the discontinuity at $x = 0$. At this point, part of the wave is transmitted to the right (A_t) and part is reflected (A_r); evanescent waves are generated to the left and right, denoted respectively by A_e^- and A_e^+.

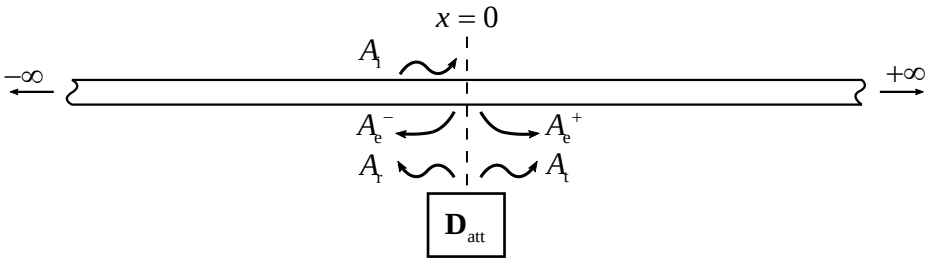

Figure 1. Infinite beam with an attached dynamic stiffness at $x = 0$ and the wave components arising from the incidence of propagating wave on the discontinuity.

The total motion of the beam is determined by the solution of the classical Euler-Bernoulli equation for beams, from which a time harmonic transverse displacement is described by $w(x,t) = \mathrm{Re}\left\{W(x)e^{j\omega t}\right\}$, where the spatial motion in the left-hand (superscript -) and right-hand (superscript +) sections of the beam is given, respectively, by

$$W^-(x) = A_i e^{-j\beta x} + A_r e^{j\beta x} + A_e^- e^{\beta x} \text{ and } W^+(x) = A_t e^{-j\beta x} + A_e^+ e^{-\beta x} \tag{1.a,b}$$

where $\beta = \sqrt{\omega}\sqrt[4]{\rho S/EI}$ is the flexural wavenumber, ω is the frequency and $j = \sqrt{-1}$. The unknown wave amplitudes are found from the equations of continuity and equilibrium at the discontinuity, where the attached element resists the motion and reacts with a force and moment proportional to the dynamic stiffness matrix $\mathbf{D}_{\text{att}}$. In this sense, at $x = 0$, the relationship of forces (F) and moments (M) applied, with transverse displacement and the slope Θ can be expressed by

$$\frac{1}{EI\beta^3}\begin{Bmatrix} F \\ M\beta \end{Bmatrix} = \begin{bmatrix} \hat{D} & 0 \\ 0 & \tilde{D} \end{bmatrix}\begin{Bmatrix} W(0) \\ \Theta(0)\beta^{-1} \end{Bmatrix}, \tag{2}$$

where $\hat{D}$ and $\tilde{D}$ are, respectively, the attachment's non-dimensional translational and rotational dynamic stiffness.

The magnitude of the wave transmitted across the discontinuity divided by the magnitude of the incident wave gives the transmission coefficient, and is given by (Mace, 1984)

$$\frac{A_t}{A_i} = \frac{4 - \hat{D} + \tilde{D}}{4 - \hat{D}(1+j) + \tilde{D}(1-j) - \frac{\hat{D}\tilde{D}}{2}} . \tag{3}$$

Essential insights into the behaviour of the beam subject to a force- and/or moment-like discontinuity can be extracted from Eq. (3). Note that if $\hat{D} = \tilde{D} = 0$ the structure is homogeneous and the transmission is free and equal to one unit. On the other hand, with the discontinuity present, the magnitude of the transmitted wave can be reduced. The effects of different lumped elements are discussed in the next subsection.

2.1 Single type of discontinuity

To illustrate the interaction of the beam with different attached elements we first consider the discontinuity that consists of a concentrated mass, such that $\tilde{D} = 0$ and $\hat{D} = -\omega^2 m / EI\beta^3 = \hat{D}_m$, which is the ratio of the mass m, to $1/2\pi$ of the beam mass with length equal to the wavelength λ. The transmission ratio for this condition is shown in Fig. 2 as function of $|\hat{D}|$ in the thick gray solid line. Note that at small values of $\hat{D}_m$, or low frequencies, the transmission tends to a unit. At large values of $\hat{D}_m$, or high frequencies, there is a maximum transmission reduction of -3 dB, i.e., $|A_t / A_i| = 1/\sqrt{2}$. Consider now that a translational grounded spring of stiffness k, that is attached to the beam, so $\hat{D} = k / EI\beta^3 = \hat{D}_k$, the transmission ratio curve takes the form shown in the thin black line in Fig. 2. In this case, for small values of $\hat{D}_k$, or high frequencies, there is no effective transmission reduction, but for large values of $\hat{D}_k$, or low frequencies, the resulting maximum transmission reduction is -3 dB. These effects can be easily interpreted assuming the discontinuity as a simple support. In that case, the transverse motion will be zero at $x = 0$, and the shear force of the incident wave will not transmit power into the right part of the beam, while power transmission via bending moment is not affected by the discontinuity, so if $\hat{D} \gg 4$ and $\tilde{D} = 0$, therefore the modulus of the transmitted wave amplitude is $1/\sqrt{2}$ the incident wave amplitude modulus. A similar effect is observed if the discontinuity prevents only rotational motion so that the bending moment of the incident wave does not transmit power.

Assume now that the discontinuity consists of a rotational grounded spring of stiffness s or a pure moment of inertia $J = m\kappa^2$ with mass m and radius of gyration κ. The non-dimensional dynamic stiffness of these elements can be written as $\tilde{D} = s / EI\beta = \tilde{D}_s$ and $\tilde{D} = -\omega^2 J / EI\beta = \tilde{D}_J$. By setting $\hat{D} = 0$ in Eq. (3), results in an algebraic equivalence for the mass and grounded spring discontinuities, respectively, when $\tilde{D} = 0$. In other words, the transmission coefficient for a mass-type discontinuity is algebraically equal to the transmission coefficient for a rotational spring-type discontinuity; and similarly, the transmission coefficients for the inertia-type discontinuity is algebraically equal to the translational spring discontinuity (Mead, 1982). Hence, the wave transmission curves for these rotational elements assume the equivalent behaviour for the translational elements shown in Fig. 2.

Figure 2 is a classic representation that allows a physical insight into the interaction between the beam and the attachment. In addition to the observations discussed above, note that the grounded line spring and the pure rotational inertia can, at a particular frequency, when $|\hat{D}| = 4$ or $|\tilde{D}| = 4$, effectively prevent all transversal and rotational motion at the point of attachment. This condition is highlighted by the dip in the transmission ratio and can be easily interpreted by setting the numerator of Eq. (3) to 0, this is

$$4 - \hat{D} + \tilde{D} = 0 . \tag{4}$$

Doing this for each of the elements, i.e., $4 - \hat{D}_k = 0$ and $4 + \tilde{D}_J = 0$, it is possible to determine that, at this condition, the spring resonates with the effective mass of the beam and the effective rotational stiffness of the beam resonates with the attached inertia.

This effective mass of the beam, which is approximately $2\rho S\lambda/\pi$, is given by the real part of the point dynamic stiffness of the infinite beam excited with a harmonic force. The effective rotational stiffness, in turn, is obtained from the real part of the point dynamic stiffness of the infinite beam excited with a harmonic bending moment and corresponds to $8\pi EI/\lambda$. These reactive elements observed in the beam's response to excitation make it possible to create a zero transmission condition without necessarily attaching a vibration neutraliser.

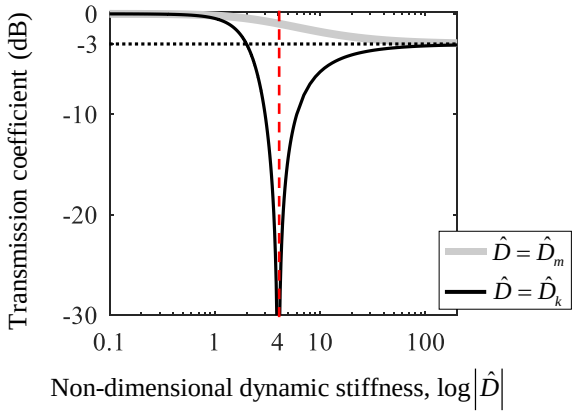

Figure 2. Transmission coefficient for beam with discontinuity consisting on a concentrated mass, thick gray line; and grounded line spring, thin black line.

3. DISPLACEMENT TRANSMISSIBILITY IN A BEAM WITH ATTACHED LUMPED ELEMENTS

The physical insight extracted from the previous wave-based analysis can also be inferred from the transmissibility analysis. In this regard, consider that the beam shown in Figure 3 that has the same material and area properties as the beam shown in Figure 1, with total length $L = 2l$. The relationship between normalised force vector $\mathbf{f}$ and displacement vector $\mathbf{u}$ is given by the dynamic stiffness matrix $\mathbf{D}$, i.e., $\mathbf{f} = \mathbf{D}\mathbf{u}$ or (Gardonio and Brennan, 2004)

$$\frac{1}{EI\beta^3}\begin{Bmatrix} F_{\mathrm{L}} \\ M_{\mathrm{L}}\beta \\ F_{\mathrm{att}} \\ M_{\mathrm{att}}\beta \\ F_{\mathrm{R}} \\ M_{\mathrm{R}}\beta \end{Bmatrix} = \frac{1}{H}\begin{bmatrix} -K_{11} & -P & K_{12} & V & 0 & 0 \\ -P & Q_{11} & -V & Q_{12} & 0 & 0 \\ K_{12} & -V & -2K_{11}+\hat{D}_k H & 0 & K_{12} & V \\ V & Q_{12} & 0 & 2Q_{11}+\tilde{D}_J H & -V & Q_{12} \\ 0 & 0 & K_{12} & -V & -K_{11} & P \\ 0 & 0 & V & Q_{12} & P & Q_{11} \end{bmatrix}\begin{Bmatrix} W_{\mathrm{L}} \\ \Theta_{\mathrm{L}}\beta^{-1} \\ W_{\mathrm{att}} \\ \Theta_{\mathrm{att}}\beta^{-1} \\ W_{\mathrm{R}} \\ \Theta_{\mathrm{R}}\beta^{-1} \end{Bmatrix}, \tag{5}$$

where $K_{11} = \cos(\beta l)\sinh(\beta l) + \sin(\beta l)\cosh(\beta l)$, $Q_{11} = \cos(\beta l)\sinh(\beta l) - \sin(\beta l)\cosh(\beta l)$, $P = \sin(\beta l)\sinh(\beta l)$, $K_{12} = \sin(\beta l) + \sinh(\beta l)$, $Q_{12} = \sin(\beta l) - \sinh(\beta l)$, $V = \cos(\beta l) - \cosh(\beta l)$ and $H = \cos(\beta l)\cosh(\beta l) - 1$. Equation (5) is normalised so that $\mathbf{D}$ becomes a non-dimensional dynamic stiffness matrix.

The non-dimensional attached dynamic stiffnesses $\hat{D}$ and $\tilde{D}$ assume the same forms as in section 2, and are positioned at the center point of the beam aiming for symmetry of the system. As discussed in the previous section, the resonant elements are assumed to consist of a translational grounded spring of stiffness $\hat{k}$, and a pure moment of inertia $J = m\kappa^2$. The non-dimensional dynamic stiffnesses are rewritten, in terms of the geometric parameters of the beam, so that

$$\hat{D}_k = \frac{k}{EI\beta^3} = \frac{\varepsilon}{(\beta L)^3} \text{ and } \tilde{D}_J = \frac{-\omega^2 J}{EI\beta} = -(\beta L)^3 \mu\gamma^2 \tag{6}$$

where $\varepsilon = k/\left(EI/L^3\right)$ is the ratio of the attached stiffness to the beam bending stiffness, $\mu = m/\rho SL$ is the ratio of the mass to the beam mass and $\gamma = \kappa/L$ is the ratio of the radius of gyration to the beam length.

Displacement transmissibility is a practical approach to evaluating the transmission of vibration between two points in a system. One of the ways to obtain the transmissibility is from the ratio between the transfer receptance and the point receptance. The receptance matrix, in turn, is described by $\mathbf{R} = \mathbf{D}^{-1}$, from which the transverse displacement transmissibility for the beam excited with a force at the left end is given by

$$\left|\frac{W_R}{W_L}\right| = |T| = \left|\frac{R_{(5,1)}}{R_{(1,1)}}\right|, \tag{7}$$

where the subscripts (5,1) and (1,1) denote the respective elements of the matrix $\mathbf{R}$. In this analysis, it is possible to determine the occurrence of the boundary frequencies, where $|T|=1$; the attenuation bands, where $|T|<1$; and where the relative response will be amplified, $|T|>1$.

Figure 4 presents the transmissibility and the respective point and transfer receptances, as expressed in Eq. (7), as a function of the dimensionless frequency $L/\lambda = \beta L/2\pi$. To control the resonance peaks, structural damping was assumed through the complex wave number $\beta' = \beta(1-j\eta/4)$, where $\eta = 0.01$ is the loss factor.

The transmissibility presented in the thick grey line refers to the host structure, while the thin black curve refers to the system when coupled with the elements expressed by Eq. (6). Assuming ε constant, the inertial device is varied between (i) and (v) by adding mass, i.e., by increasing μ. The vertical dashed lines follow the dips in the transmissibility, which correspond to the anti-resonances in the transfer receptance. In (i) the dip that occurs at low frequencies is controlled by the spring, while the dip observed at high frequencies is controlled by the moment of inertia. Note that increasing mass results in shifting of both dips until the effects collapse, as shown in (iv). The conditions in (ii) and (iii) present special situations where the dip controlled by the spring and by the inertia, respectively, disappear due to a receptance match, a phenomenon previously studied and presented as a super attenuation band or super stop band (Cleante et al., 2022; Germanos Cleante et al., 2023). After the collapse of the dips in (iv) the increase in mass implies the suppression of the effect, hence no dip is observed in (v).

To interpret the behaviour observed in Figure 4(v), Figure 5 presents the transmissibility for three different systems. The thick solid line corresponds to the structure with the grounded spring and moment of inertia attached. The dashed transmissibility curve corresponds to the structure with moment of inertia but with a pin support instead of a spring. Similarly, the thin dash-dot line corresponds to the system with a grounded spring and sliding support instead of the moment of inertia. The comparative behaviour of the curves shows that after the collapse of the dips, the transmissibility is controlled at low frequencies by the stiffness of the spring, behaving as a pinned support, and at high frequencies by the inertia, behaving as a sliding support. This is in line with the discussions presented in section 2. Whether it is, a large mass or a very stiff spring, at large values of $\hat{D}_k$ and $\tilde{D}_J$ all motion associated with the respective discontinuity, transverse or rotational, is constrained and therefore behaves like a pinned or sliding support.

In order to further investigate the advantages of the studied structure, it is possible, with the adjustment of the properties of the coupled elements, to obtain an ultra-wideband of attenuation, shown in Figure 6. As previously mentioned, this phenomenon occurs in a match of receptances highlighted by vertical dashed lines. It is observed that the anti-resonance of the transfer receptance, which is mainly controlled by the coupled spring – since the dynamic stiffness of this element is dominant at low frequencies – coincides with the anti-resonance of the point receptance; while the anti-resonance is mainly controlled by the moment of inertia – since the dynamic stiffness of this element is dominant at high frequencies – merges with the resonance of the transfer receptance and coincides with the resonance of the point receptance. This superposition of modes results in this smooth attenuation band effect on transmissibility. In this case there are two tuning conditions occurring so that the attenuation region formed has a greater bandwidth than the super attenuation band in Figure 4, thus being called a hyper attenuation band (HAB). It is worth mentioning that this result requires robust tuning and obtaining the necessary parameters for this can be difficult, therefore requiring a deeper investigation.

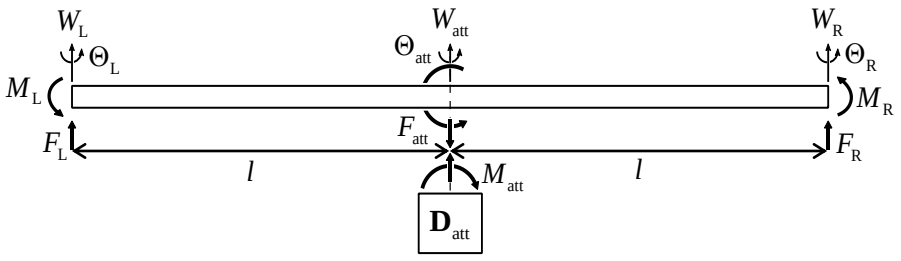

Figure 3. Finite beam with an attached discontinuity at the centre point “att”.

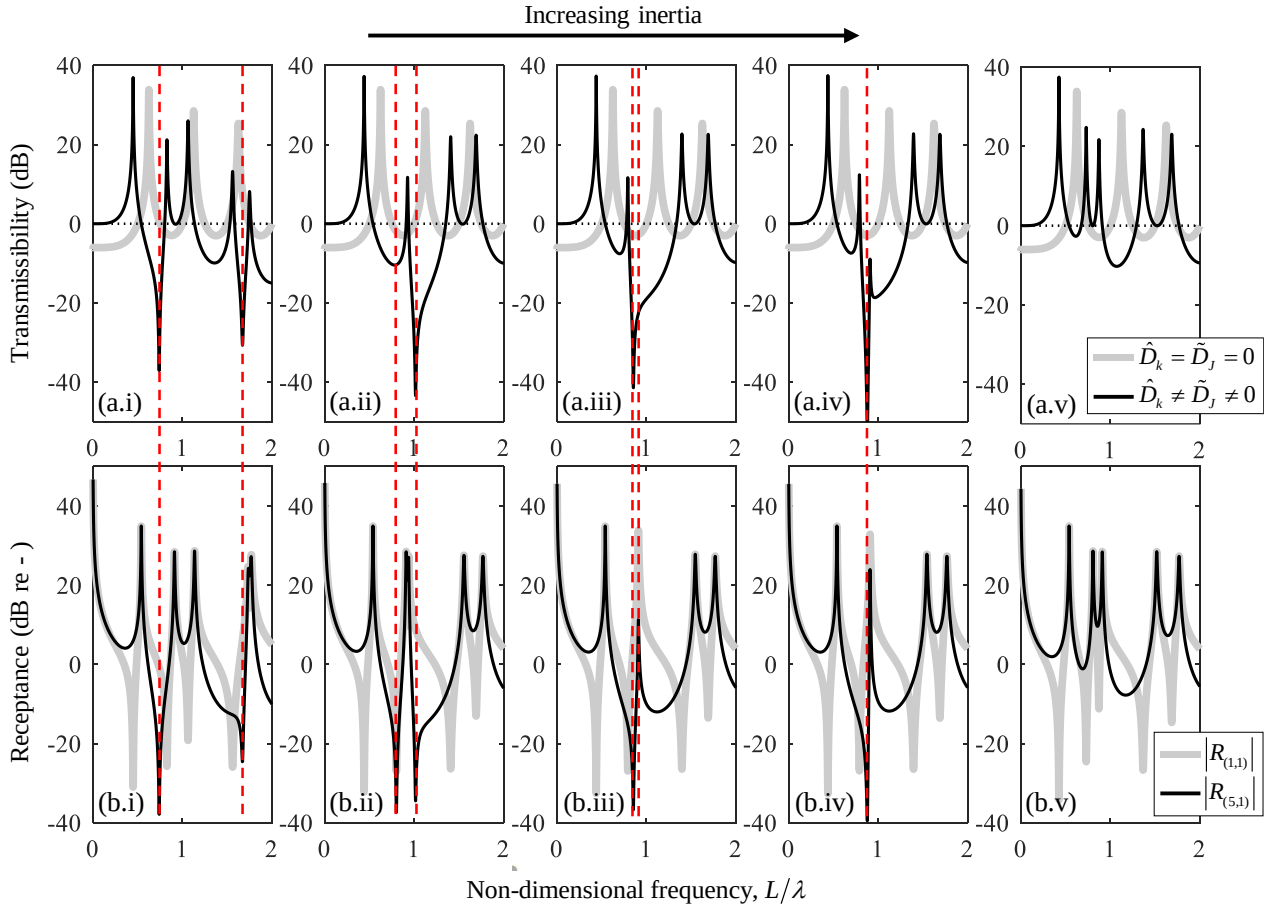

Figure 4. Response for beam system with grounded spring and pure moment of inertia. (a) Transmissibility, bare beam, thick gray line; and system, thin black line. (b) System driving point receptance, thick gray line; and system transfer receptance, thin black line. Assuming $\varepsilon = 300$, $\gamma = 0.2$ and (i) $\mu = 0.08$, (ii) $\mu = 0.325$, (iii) $\mu = 0.388$, (iv) $\mu = 0.394$, (v) $\mu = 0.8$.

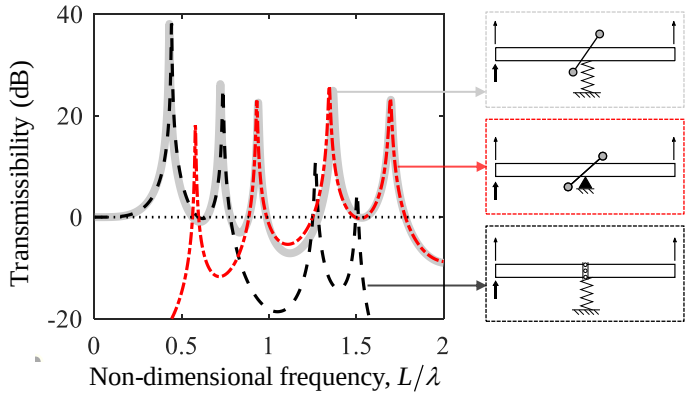

Figure 5. Displacement transmissibility for different coupling systems. Translational grounded spring and pure moment of inertia, gray solid line; pure moment of inertia and pinned support, dashed line; and translational grounded spring and sliding support, dash-dot line. Assuming $\varepsilon = 500$, $\gamma = 0.2$ and $\mu = 1$.

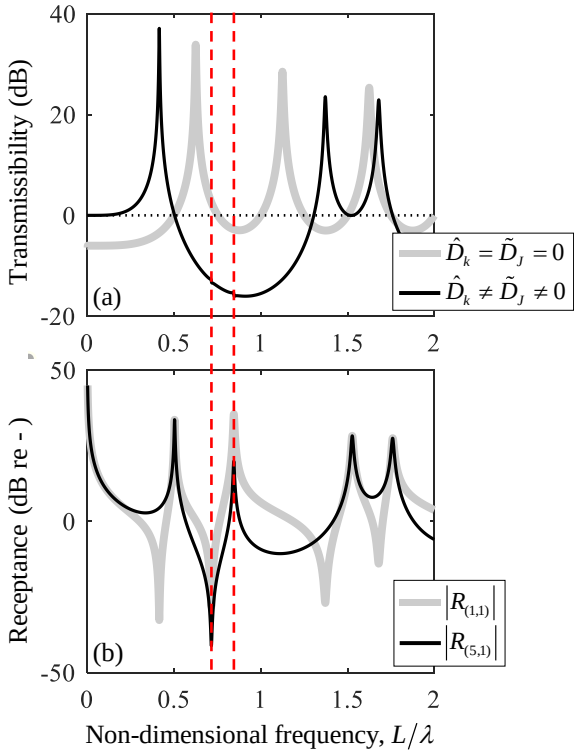

Figure 6. Response for beam system with grounded spring and pure moment of inertia adjusted to form a hyper attenuation band. (a) Transmissibility, bare beam, thick gray line; and system, thin black line. (b) System driving point receptance, thick gray line; and transfer receptance, thin black line. Assuming $\varepsilon = 163$, $\gamma = 0.2$ and $\mu = 0.6045$.

4. EXPERIMENTAL DEMONSTRATION

Laboratory-based experiments were conducted to support the theoretical investigation. The system consists of a 1500 x 12 x 3 mm long single span aluminium beam with Young's modulus $E = 66$ GPa and density $\rho = 2700$ kg/m^3, in which two types of devices are attached at its central point: a rotary inertia and a grounded translational spring.

The beam was suspended vertically by thin wires to simulate free-free boundary conditions. Two accelerometers PCB type 352C23 were attached to the host beam's upper (W_L) and lower (W_R) ends and a PCB type 086E80 impact hammer was used to excite the structure. The data was recorded using a Data Physics QUATTRO mobile system, and the point and transfer transverse accelerances were calculated using the SignalCalC 900 Series software by averaging the measurements from 10 impacts with 6400 spectral lines and a sampling frequency of 500 Hz. The transmissibility was calculated from the ratio of the measured transverse accelerances.

The rotational device consists of two aluminium tubular arms connected through the beam by a screw, as shown in Figure 7(a). The device has the same material properties as the host beam, with an outer diameter of 6.3 mm and an inner diameter of 3.8 mm, which allows calculating the second moment of area I_{tube} and the cross-sectional area S_{tube}. A group of nuts and washers make up the mass at the ends of the arm m_{end}. The tuning frequency can be adjusted by changing the arm length and/or the mass at the ends.

The dynamic stiffness of the rotary inertia deviates from the theory, not behaving as a concentrated element and expressed by Eq. (6). In real elements it is assumed to be a continuous system, modelled as a beam subject to shear forces, bending moments and axial forces. The latter corresponds to the shear force on the host beam. The dynamic stiffness matrix for this device is $\mathbf{D}_{\text{att}} = \mathbf{K} - \omega^2\mathbf{M}$, where the mass and stiffness matrices, for the element of length l_{tube}, defined from finite element method are (Petyt, 2010)

$$\mathbf{M} = \frac{1}{420}\begin{bmatrix} 140(3m_{\text{c}} + m_{\text{tube}}) & 0 & 0 & 0 & 0 \\ 0 & 0 & 0 & 0 & 0 \\ 0 & 0 & 140(3m_{\text{end}} + m_{\text{tube}}) & 0 & 0 \\ 0 & 0 & 0 & 12(35m_{\text{end}} + 13m_{\text{tube}}) & 0 \\ 0 & 0 & 0 & 0 & 0 \end{bmatrix} \tag{8}$$

and

$$\mathbf{K} = \frac{EI_{\text{tube}}}{l_{\text{tube}}^{\,3}} \begin{bmatrix} S_{\text{tube}} l_{\text{tube}}^{\,2} / I_{\text{tube}} & 0 & -S_{\text{tube}} l_{\text{tube}}^{\,2} / I_{\text{tube}} & 0 & 0 \\ 0 & 4l_{\text{tube}}^2 & 0 & -6l_{\text{tube}} & 2l_{\text{tube}}^2 \\ -S_{\text{tube}} l_{\text{tube}}^{\,2} / I_{\text{tube}} & 0 & S_{\text{tube}} l_{\text{tube}}^{\,2} / I_{\text{tube}} & 0 & 0 \\ 0 & -6l_{\text{tube}} & 0 & 12 & -6l_{\text{tube}} \\ 0 & 2l_{\text{tube}}^2 & 0 & -6l_{\text{tube}} & 4l_{\text{tube}}^2 \end{bmatrix}, \tag{9}$$

where $m_{\text{tube}} = \rho S_{\text{tube}} l_{\text{tube}}$ is the tube mass and m_{c} is a point mass due to the device's coupling to the host beam. It was assumed that the axial motion in the part coupled to the host beam is negligible. Furthermore, note that the terms in the mass matrix, much smaller than 1/3 of the tube mass were neglected. This approach allows, after some mathematical manipulations, to approximate the dynamic behaviour of the device to a single degree of freedom. Therefore, the approximate translational and rotational dynamic stiffnesses will be given, respectively, by

$$\hat{D}_{\text{eq}} \approx -\frac{1}{EI\beta^3}\omega^2 \left(m_{\text{tube}} + 3m_{\text{c}}\right) \tag{10}$$

and

$$\tilde{D} \approx \frac{1}{EI\beta}\frac{-\omega^2 J_{\text{eq}} s_{\text{eq}}}{3s_{\text{eq}} - \omega^2 J_{\text{eq}}}. \tag{11}$$

Equation (11) represents the dynamic stiffness of an equivalent moment of inertia $J_{\text{eq}} = \left(m_{\text{tube}} + 3m_{\text{end}}\right) l_{\text{tube}}^2$ in series with the stiffness of the arm $s_{\text{eq}} = 3EI_{\text{tube}} / l_{\text{tube}}$. Given $l_{\text{tube}} = 158.6$ mm, the equivalent value of γ is about 0.106.

The grounded spring was produced by a PVC ring 104 mm in diameter and 3.1 mm in thickness, in which one end was fixed on the experiment bench and the opposite end connected to the host beam – see Fig. 7(a). A hinge prototyped by 3D printing, glued between the ring and the beam, ensures that the ring interacts only in the transverse motion and maintains free rotational motion, in addition to allowing free operation of the beam-like moment resonator.

The translational attached dynamic stiffness is given by the sum of the transverse effect of the moment resonator (Eq. (10)) and the dynamic stiffness of the grounded spring, and is expressed as

$$\hat{D} = \frac{1}{EI\beta^3}\left[-\omega^2 \left(m_{\text{tube}} + 3m_{\text{c}}\right) + k\right]. \tag{12}$$

The ring stiffness k is estimated by solving the dimensional form of Eq. (4), assuming $\omega = \omega_{\text{dip}} = 2\pi f_{\text{dip}}$, this is, solving $4 - \hat{D} / EI\beta_{\text{dip}}^3 = 0$, where β_{dip} is the beam wavenumber at ω_{dip}. The dip frequency f_{dip} is obtained from the anti-resonance of the experimental transfer accelerance only with the ring attached. Hence, the stiffness ratio is estimated as $\varepsilon = k / EI\beta_{\text{dip}}^3 = 5.61$. The concentrated coupling mass is $m_{\text{c}} = 6.8$ g, being composed by the screw and the hinge masses, as well as $m_{\text{tube}} = 9.9$ g and $m_{\text{end}} = 5.76$ g. The ring mass is neglected. Therefore, the equivalent mass ratio is given by $\mu = \left(m_{\text{c}} + m_{\text{end}} + m_{\text{tube}}\right) / \text{beam mass} \approx 0.15$.

Figure 7(b) shows the comparison between experimental and theoretical results for transverse transmissibility. The solid grey and thin black curves represent the experimental and prediction results, respectively. By matching the experimental data with the model, the material loss factor of the beam, the spring and the beam-like moment attachment are found to be, respectively, 0.005, 0.07 and 0.15. The curves present good agreement. The dashed vertical lines indicate the experimental dip frequencies. The first occurs at approximately 90.5 Hz, while the prediction is 88.7 Hz. The second experimental dip frequency occurs at 209.4 Hz and the predicted value is 200.3 Hz.

These results qualitatively demonstrate the character of the discussed effects, however grounded springs are not suitable in most practical applications. In this sense force neutralizers are potentially more suitable to obtain the phenomena presented in section 3 in real structures. To form the HAB, precise tuning of both devices is necessary, however, the constructive limitations of the PVC ring and the moment resonator made the experimental observation of this phenomenon unfeasible. The blue dotted line in Fig. 7 shows the transmissibility resulting from the robust tuning of the devices and the HAB formed between the frequencies of 120 Hz and 224 Hz. To obtain the same result experimentally it is necessary to increase the ring stiffness by approximately 56% and reduce the equivalent moment of inertia approximately in 1.7%.

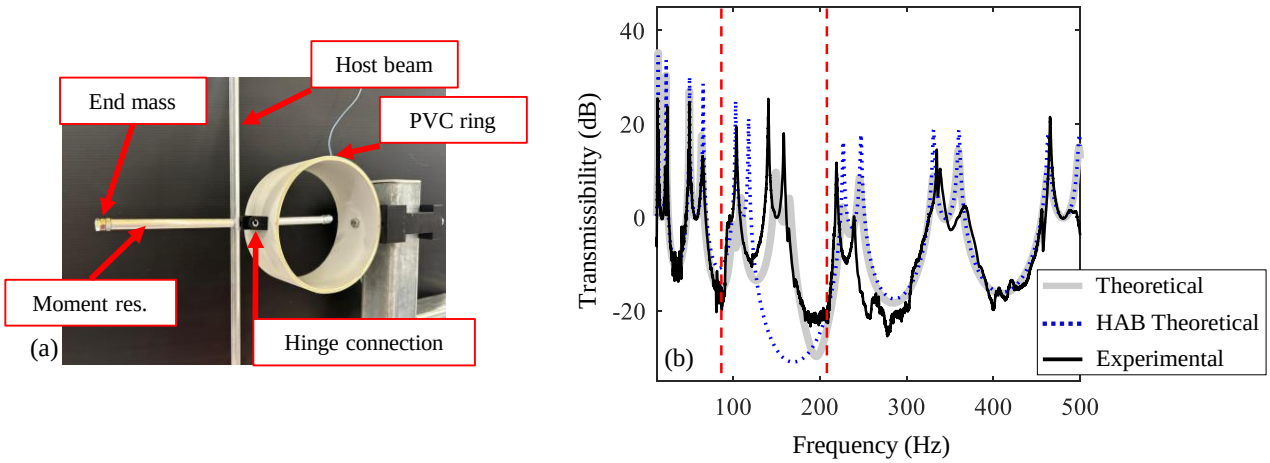

Figure 7. Experimental disposition and results. (a) Experimental device setup. (b) comparison between transversal displacement transmissibilities measured, blrack thin solid line, and predicted by Eq. (7), grey thin solid line. Dotted line illustrates the condition under which the hyper attenuation band is formed.

5. CONCLUSIONS

The effect of lumped elements attached to infinite and finite beams was evaluated in this work. The transmission coefficient was determined using a wave-based approach and through the dynamic stiffness matrix method the transmissibility of displacements was obtained. The discussions showed that a zero transmission can be obtained by the resonant interaction of the beam with systems with transverse stiffness-like or rotational mass-like behaviour, that is in agreement with past results in the literature. Aiming for simplicity and physical interpretation of the numerical analyses, the attachment of a transverse grounded spring and a pure moment of inertia to a finite slender beam was considered in details. The results indicate different advantageous conditions in terms of transmitted vibration attenuation. First, the emergence of dips in transmissibility at low and high frequencies is highlighted, being controlled separately by each of the attached devices. The second aspect concerns using different combinations to form of a super attenuation band, a region characterized by a smooth transmissibility curve and a bandwidth greater than the bandwidth of the local resonant effect. However, these conditions will not be observed when the combined stiffness of the external discontinuity acts in such a way that the coupled elements behave as pinned and sliding supports, respectively. The theoretical developments were demonstrated by experimental results.

6. ACKNOWLEDGEMENTS

The authors acknowledge the financial support of the São Paulo Research Foundation (FAPESP), grant numbers 2018/15894-0, 2019/19335-9, 2022/11995-2; 2022/09543-6 and 20/00534-9; the National Council for Scientific and Technological Development (CNPq), grant numbers 406594/2021-0 and 407152/2022-9; and the University of Auckland - Education New Zealand, “Controlling structure-borne noise propagation using arrays of periodic elements”, 3720928.

7. REFERENCES

Brennan, M.J., 1999, “CONTROL OF FLEXURAL WAVES ON A BEAM USING A TUNABLE VIBRATION NEUTRALISER:” Journal of Sound and Vibration, v. 222, no. 3, p. 389–407.

Chen, S., Yang, Z., Ying, M., Zheng, Y., Liu, Y., and Pan, Z., 2020, “Parallel Load-Bearing and Damping System Design and Test for Satellite Vibration Suppression:” Applied Sciences, v. 10, no. 4, p. 1548.

Cleante, V.G., Brennan, M.J., Gonçalves, P.J.P., and Carneiro, J.P., 2022, “On the formation of a super stop-band in finite mono-coupled periodic structures using an array of vibration absorbers: Controlling parameters and physical insight:” Mechanical Systems and Signal Processing, v. 180.

Cremer, L., Heckl, M., and Petersson, B.A.T., 2005, “Structure-borne sound: Structural vibrations and sound radiation at audio frequencies:” Springer, Berlin. Germany, 1–607 p.

Gardonio, P., and Brennan, M.J., 2004, “Mobility and impedance methods in structural dynamics,” *in* Fahy, F. and Walker, J. eds., Advanced Applications in Acoustics, Noise and Vibration: Spon Press, London, p. 389–447.

Germanos Cleante, V., Brennan, M.J., Paupitz Gonçalves, P.J., and Carneiro, J.P., 2023, “On the Formation of a Super Attenuation Band in a Mono-coupled Finite Periodic Structure Comprising Asymmetric Cells,” *in*, p. 703–712.

Jafari, M., and Alipour, A., 2021, "Methodologies to mitigate wind-induced vibration of tall buildings: A state-of-the-art review:" Journal of Building Engineering, v. 33, p. 101582.
Jiménez-Alonso, J.F., Naranjo-Perez, J., Díaz, I.M., and Sáez, A., 2020, "Motion-based design of vibrating civil engineering structures under uncertainty conditions:" Structural Concrete, v. 21, no. 6, p. 2339–2352.
Kalderon, M., Mantakas, A., Paradeisiotis, A., Antoniadis, I., and Sapountzakis, E.J., 2022, "Locally resonant metamaterials utilizing dynamic directional amplification: An application for seismic mitigation:" Applied Mathematical Modelling, v. 110, p. 1–16.
Mace, B.R., 1984, "Wave reflection and transmission in beams:" Journal of Sound and Vibration, v. 97, no. 2, p. 237–246.
Mead, D.J., 1982, "Structural wave motion," *in* White, R.G. and Walker, J.G. eds., Noise and Vibration: Ellis Horwood, Southampton, p. 207–226.
Mead, D.J., 1998, "Passive vibration control:" Wiley, 540 p.
Meskouris, K., Butenweg, C., Hinzen, K.-G., and Höffer, R., 2019, "Structural Dynamics with Applications in Earthquake and Wind Engineering:" Springer Berlin Heidelberg, Berlin, Heidelberg.
Petyt, M., 2010, "Introduction to Finite Element Vibration Analysis:" Cambridge University Press.
Toit, D. du, Mace, B., Sorokin, V., and Rughunanan, L., 2021, "Control of bending wave transmission through an uncoupled force and moment neutraliser:" Journal of Sound and Vibration, v. 508, p. 116219.

8. RESPONSIBILITY NOTICE

The authors are the only responsible for the printed material included in this paper.